Chemical Engineering Journal 296 (2016) 377–385

Contents lists available at ScienceDirect

Chemical Engineering Journal

journal homepage: www.elsevier.com/locate/cej

Investigation of multiphysics in tubular microbial fuel cells by coupled computational fluid dynamics with multi-order Butler–Volmer reactions

Lei Zhao [a,1], Jian Li [b,1], Francine Battaglia [a,*], Zhen He [b,*]

[a] Department of Mechanical Engineering, Virginia Polytechnic Institute and State University, Blacksburg, VA 24060, USA
[b] Department of Civil and Environmental Engineering, Virginia Polytechnic Institute and State University, Blacksburg, VA 24060, USA

HIGHLIGHTS

- A coupled CFD-multi order Butler Volmer reaction model is developed.
- Surface reaction rate is proportional to substrate with a reaction order of 6.4.
- The coupled model can well predict current generation.
- Convective flow conditions and heterogeneous species distributions are simulated.

GRAPHICAL ABSTRACT

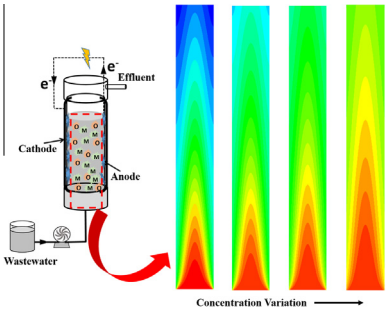

ARTICLE INFO

Article history:
Received 8 January 2016
Received in revised form 21 March 2016
Accepted 22 March 2016
Available online 28 March 2016

Keywords:
Microbial fuel cell
Computation fluid dynamics
Multi-order reactions
Wastewater treatment
Heterogeneous distribution

ABSTRACT

Microbial fuel cells (MFCs) are considered as an emerging concept for sustainable wastewater treatment with energy recovery. The anode of an MFC plays a key role in conversion of organic compounds to electricity, and thus understanding the multiphysics within the anodic compartment will be helpful with MFC optimization and scaling-up. In this study, a multi-order Butler–Volmer reaction model was proposed to compute organic consumption and energy recovery. Computational fluid dynamics (CFD) was applied to analyze the hydrodynamics and species transport inside the anodic compartment. By comparing to the experimental data, the reaction order of anodic surface reaction was determined as 6.4. The reaction model gave good agreement with experimental data when the influent sodium acetate was 1.0, 0.5 and 0.3 g L^{-1} at anodic hydraulic retention time (HRT) of 10 h, indicating the effectiveness of this multi-order Butler–Volmer reaction model. When the influent sodium acetate was 0.2 g L^{-1} or the anodic HRT was 15 h, the model exhibited discrepancies in predicting current generation and effluent chemical oxygen demand (COD) concentration, likely due to the interference of the decayed biomass and the activities of non-electroactive bacteria. The results of this study have demonstrated the viability of coupling CFD with a multi-order reaction model to understand the key operating factors of an MFC.

1. Introduction

Microbial fuel cells (MFCs) have emerged as a promising approach for sustainable wastewater treatment with bioenergy recovery [1]. In MFCs, organic materials are biologically degraded and electrical energy is produced through interaction between microbes and solid electron acceptors [2]. Various configurations of MFCs have been developed to optimize organics removal, energy recovery and operational flexibility [3–6]. Among these proposed configurations, tubular MFC systems have been studied in great detail because of its potential advantages in microbial and substrate distribution, short distance between anode and cathode electrodes, and large surface area of separator materials [7–10].

* Corresponding authors. Tel.: +1 (540) 231 0077 (F. Battaglia), +1 (540) 231 1346 (Z. He).
E-mail addresses: fbattaglia@vt.edu (F. Battaglia), zhenhe@vt.edu (Z. He).
[1] Those authors contributed equally.

http://dx.doi.org/10.1016/j.cej.2016.03.110
1385-8947/

Interdependent multiphysics processes are present in tubular MFCs. For example, the hydrodynamics of electrolyte flow in the anodic chamber plays a key role in the substrate transport with associated effects on the activation overpotential distribution and chemical reactions, and vice versa. The activation overpotential and chemical reactions could contribute to the substrate consumption and transport, thereby impacting the flow field. Therefore, proper understanding of multiphysics phenomena in tubular MFCs can help guide the design and operation of such systems.

Mathematical modeling is a powerful tool to complement experiments and can be used to further understand the key processes that cannot be easily measured via experiments. Several models have been developed for studying metabolic pathway in anaerobic mixed culture fermentation and MFCs [11–13], and among them, computational fluid dynamics (CFD) can be used to numerically predict fluid flow, including mass transfer and reactions by solving various advection–diffusion equations. The application of CFD techniques in studying MFCs is still limited with very few publications in the past ten years. An early study combined MATLAB, COMSOL and a self-developed Java code to study the macro-scale homogeneous concentration evolution of soluble substrates and biomass in bulky liquid, and a micro-scale heterogeneous two dimensional biofilm model [14]. In this model, liquid velocity was calculated from the Navier–Stokes equations within a laminar flow regime, and it was found that localized proton accumulation was a rate-limiting factor on MFC output, and porous bio-electrode did not necessarily generate higher current as long as convective flow was absent. Unfortunately, those findings were not substantiated by any experimental results. Numerical simulations using CFD-ACE + demonstrated in a Y-shape mixer with inset cylinders, a lower aspect ratio (micro-channel depth-to-width) and larger inlet Reynolds number ratio (Reynolds number ratio based on inlet streams) could enhance flow mixing efficiency, due to the increased side wall effect and shear stress [15]. COMSOL Multiphysics was used to simulate laminar incompressible fluid flow in an MFC and demonstrated that enlarged biofilm attachment and increased shear rate within helical flow pathways accounted for the enhanced MFC performance [16]. Subsequently, three different helical flow channels (1.5, 5.4 and 10.8 mm, based on the spacing between helices) were experimentally investigated with a maximum power density of 11.63 W m^{-3} achieved in the smallest channel, which was confirmed by CFD modeling using a two layer k–ε eddy viscosity turbulence model [17]. A recent study simulated a cubic-shaped MFC containing twelve different internal structures (e.g., triangular/rectangular shape, number, length and upward/downward orientation) using ANSYS CFX [18]. Numerical results demonstrated that the maximum power density of 0.54 W m^{-2} could be achieved with the largest working space of 0.57 m^2. The CFD prediction using ANSYS Fluent 12.1 revealed that better water distribution and biomass attachment could be developed with granular graphite and stainless steel meshes due to the minimized occurrence of preferential flow ways [19].

Although the aforementioned CFD-based MFC studies have provided useful information to understand MFC systems by analyzing micro- or macro-scaled flow conditions, there are still limitations with the CFD modeling that can be further addressed. For example, analyzing flow conditions alone fails to provide any information on activation overpotential and organic distribution, which can determine anodic surface reaction rate. A simplified electron transfer mechanism (e.g., external mediators) could be applied to electrochemically-active bacteria, which exists in a complex microbial community within the anodic chamber. Furthermore, time-dependent experimental data are essential to validate the model formulation. Herein, a coupled CFD with multi-order Butler–Volmer reaction model was proposed and validated to address some of the limitations, including a simple electron transfer mechanism, and an interaction between heterogeneous substrate and overpotential distribution on the anode surface. A direct contact electron transfer mechanism between microbes and the electrode surface was applied instead of an external mediator, because adding external mediator would not be feasible in wastewater treatments. Heterogeneous species distribution and electricity generation was predicted using the Butler–Volmer equations to include species concentration and activation overpotential on reaction rates. Real time-dependent experimental results were used for model validation. The results of this work were expected to demonstrate the viability of using a high-fidelity CFD approach to model the complex reaction physics in a tubular MFC.

2. Materials and methods

2.1. MFC setup and operation

The MFC was constructed as a tubular reactor (32 cm long and 3.8 cm inner diameter) made of anion exchange membrane (AEM-Ultrex AMI 7001, Membrane International. Inc, Glen Rock, New Jersey, USA), as shown in Fig 1. Carbon cloth (Zoltek Corporation, St. Louis, MO, USA) was used as the material for both the anodic and cathodic electrodes. Before use, the carbon cloth was soaked in acetone solvent overnight and then heated for 30 min at 450 °C. The finished anode electrode (with effective surface dimensions of 22 cm-long and 2.9 cm-diameter) was installed along the inner surface of the AEM tube and supported by a plastic mesh, resulting in a net anodic liquid volume of 350 mL. The cathode electrode (23 cm × 12 cm) was coated with Pt/C powder (Etek, Somerrest, NJ, USA) at a loading rate 0.3 mg Pt cm^{-2}, and wrapped the AEM tube. The anode and cathode electrodes were connected to a 10 Ω resistor.

The MFC was operated at room temperature. Its anodic compartment was inoculated with anaerobic sludge from the Peppers Ferry Wastewater Treatment Plant (Radford, VA, USA) and operated with sodium acetate in a batch mode. During the start-up period, the external resistance was changed from 1000 to 10 Ω in a stepwise approach. After start-up, the system was fed with a synthetic solution containing (per L of tap water): sodium acetate 1 g (otherwise stated); NH_4Cl 0.15 g; NaCl 0.5 g; $MgSO_4$ 0.015 g; $CaCl_2$ 0.02 g; KH_2PO_4 0.53 g; K_2HPO_4 1.07 g; and 1 mL trace elements [5]. No recirculation was applied to the anolyte, but the catholyte (50 mM phosphorus buffer solution) was recirculated at 5 mL min^{-1}. The catholyte was stored in a separate container (beneath the MFC reactor) and pumped to rinse the cathode surface constantly. The flowrate of the anolyte was controlled by a peristaltic pump to achieve the desired hydraulic retention time (HRT) of 10 h (otherwise stated). The Reynolds number is 0.42 based on the inlet velocity of 1.44×10^{-5} m s^{-1}.

2.2. Measurements and analysis

The MFC voltage was recorded every 5 min by a digital multimeter (2700, Keithley Instruments, Cleveland, OH). The pH was measured using a benchtop pH meter (Oakton Instruments, Vernon Hills, IL, USA). The conductivity was measured by a benchtop conductivity meter (Mettler-Toledo, Columbus, OH, USA). The concentration of chemical oxygen demand (COD) was measured by using a colorimeter according to the manufacturer's procedure (Hach DR/890, Hach Company, Loveland, CO, USA).

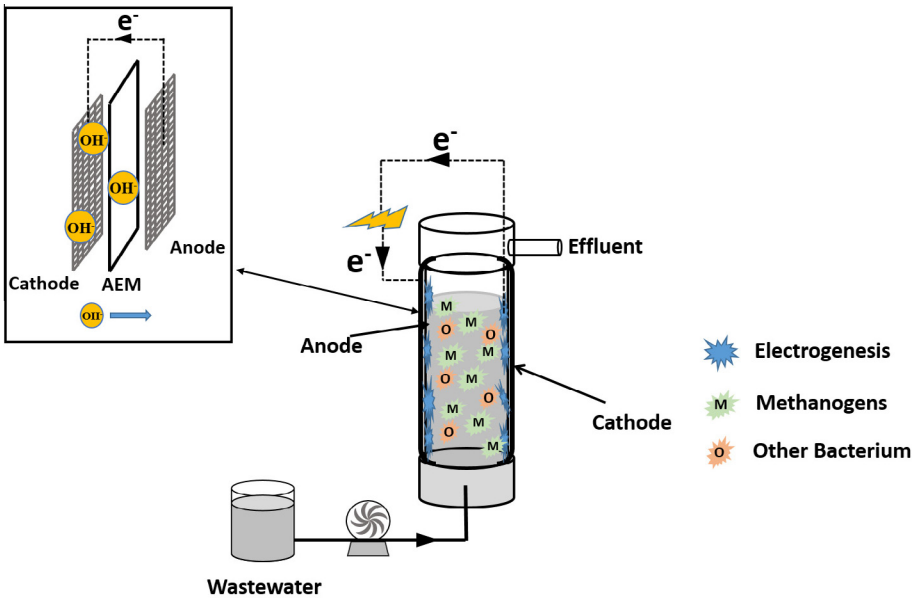

Fig. 1. A schematic of a tubular microbial fuel cell (MFC) system used for developing the CFD-multi-order Butler Volmer reaction model. Inset: enlarged arrangement of electrodes and anion exchange membrane.

3. Model formulation

3.1. Governing equations

For steady-state, laminar, incompressible flow, the continuity equation is

$$\nabla \cdot \vec{V} = 0 \tag{1}$$

where $\vec{V}$ is the velocity vector. The corresponding momentum equations for a Newtonian fluid are

$$\rho \vec{V} \nabla \cdot \vec{V} = -\nabla p + \mu \nabla^2 \vec{V} + \rho \vec{g} \tag{2}$$

From left to right, the terms represent the momentum change in a control volume due to convection, pressure gradients, viscous diffusion, and gravity. In Eqs. (1) and (2), the fluid properties, i.e., density ρ and dynamic viscosity μ, are calculated as volume-weighted mixture properties. However, due to the negligible amount of soluble substances and biomass in the bulk liquid, it is reasonable to assume that the mixture properties are equal to those of liquid water.

The heterogeneous species distribution is obtained by solving the species transport equation. For species k, the steady-state transport equation is given as:

$$\vec{V} \cdot \nabla C_k = D_k \nabla^2 C_k + S_k \tag{3}$$

The terms in Eq. (3), from left to right, represent the molar concentration change in a control volume due to convection, diffusion and reactions, respectively. The reaction term can be further expressed as the summation of a series of reactions:

$$S_k = \sum_i r_{k,i} \tag{4}$$

where $r_{k,i}$ represents the production/consumption of species k in reaction i.

Because the flow under consideration is very laminar with a Reynolds number less than 1, the flow is assumed axisymmetric. The computational domain is discretized using a rectangular mesh with dimensions of 0.22 m × 0.145 m. A Dirichlet boundary condition is applied to the inlet with a fixed velocity (1.44×10^{-5} m s^{-1} for the base case) and sodium acetate concentration (0.5 g L^{-1} for the base case). The anode surface is modeled as a no-slip wall with surface reactions accounting for the mass flux. Fully developed flow, which implies zero gradient of velocity and species, is adopted at the outlet with a gage pressure of zero.

Fixed point iteration is used to solve the nonlinear system described using Eqs. (11)–(18), and is easy to implement into CFD calculations. However, the solution procedure requires strong under relaxation to ensure convergence. A finite volume method is used to discretize the governing equations using the commercial code ANSYS Fluent 15.0. User Defined Functions (UDF) are employed to incorporate correlations for the reaction rates.

3.2. Reaction models

In an effort to reduce the associated uncertainties in modeling bacterial activities, a two-population bacterium (methanogens and electrochemically-active microorganisms) community is assumed in the anode compartment.

3.2.1. Volumetric reactions

Given the fact that various populations of bacteria exist in the bulk liquid, it is not easy to model each bacteria population separately. For simplicity, the microbes in the bulk liquid are simplified as the methanogens, which act as the catalysts in the methanogenesis process, where

$$Acetate \xrightarrow{Methanogens} CH_4 + CO_2 \tag{5}$$

The methanogens are assumed to be uniformly distributed in the bulk liquid, and in this case the conventional Monod-limitation equation is applied to approximate the reaction rate as:

$$r_v = r_{v,0} \frac{C_{ac}}{C_{ac} + K_{ac}} \tag{6}$$

3.2.2. Anodic reaction

Electrochemically-active bacteria are assumed to be evenly distributed on the anode surface. A generalized oxidation reaction

catalyzed by electrochemically-active microorganisms (electrogens) is proposed [20] and represented as:

$$CH_3COO^- + 4H_2O \xrightarrow{electrogens} 2HCO_3^- + 9H^+ + 8e^- \quad (7)$$

Eq. (7) is a chain-reaction and involves a series of sub-reactions. Based on the theory of reaction kinetics, the reaction rate of such a chain-reaction is determined in the following form:

$$r_a = kC_{ac}^{\gamma}C_{H_2O}^{\beta} \quad (8)$$

where superscripts γ and β are not necessarily equal to the stoichiometric coefficient, but the summation of γ and β defines the reaction order. The sub-reactions involved are regarded as the elementary equations, whose reaction orders equal the summation of the stoichiometric coefficients of reactants. Focusing on the acetate removal and current generation, it is reasonable to use such a generalized reaction and corresponding reaction rate formula. In addition, given that the concentration of liquid water is constant, the reaction rate is then solely related to the concentration of acetate:

$$r_a = kC_{ac}^{\gamma} \quad (9)$$

where k is the rate constant and can be calculated as the function of activation overpotential η_{act}, temperature T and transfer coefficient α from Butler–Volmer equation [21]:

$$k = r_{a,0}\left(\exp\left(\frac{\alpha F\eta_{act}}{RT}\right) - \exp\left(\frac{(\alpha-1)F\eta_{act}}{RT}\right)\right) \quad (10)$$

Combining Eqs. (9) and (10) provides an estimate of the reaction rate of the anodic reaction:

$$r_a = r_{a,0}C_{ac}^{\gamma}\left(\exp\left(\frac{\alpha F\eta_{act}}{RT}\right) - \exp\left(\frac{(\alpha-1)F\eta_{act}}{RT}\right)\right) \quad (11)$$

The relationship between reaction rate and current density is given:

$$i = nFr_a \quad (12)$$

where n is the stoichiometric coefficient of electrons in Eq. (7) and $n = 8$.

3.3. Electricity generation

The generated current can be obtained by integrating current density on the entire anode surface:

$$I = \int idA \quad (13)$$

According to Ohm's Law, cell voltage is determined when the current passes through electrical resistance:

$$V = IZ_{ext} \quad (14)$$

The cell voltage is also the difference between the open circuit voltage (OCV) and the potential loss through internal resistance,

$$V = \mathrm{OCV} - IZ_{int} \quad (15)$$

where OCV is the theoretical potential difference between the anodic and cathodic electrodes:

$$\mathrm{OCV} = E_c - E_a \quad (16)$$

It should be noted that because the cathodic performance is beyond the scope of this study, the cathodic potential (i.e., oxygen reduction reaction) is fixed at 0.3 V (vs. Standard Hydrogen Electrode). However, the anodic potential can vary due to the concentration deviation. Activation polarization occurs to overcome the energy barriers when electrons are transferred from electrode donors to acceptors, *e.g.* acetate to anode. Hence, the anodic potential is given as:

$$E_a = E_{a,0} - \frac{RT}{8F}\ln\left(\frac{C_{ac}}{C_b^2C_p^9}\right) + \eta_{act} \quad (17)$$

In summary, cell voltage can be represented as the summation of standard potential and irreversible losses,

$$V = E_c - E_{a,0} + \frac{RT}{8F}\ln\left(\frac{C_{ac}}{C_b^2C_p^9}\right) - \eta_{act} - IZ_{int} \quad (18)$$

The internal resistance (Z_{int}) is constant due to the negligible resistance of the conducting wires and high solution conductivity. From Eq. (18), concentration loss (third term on the right side) is mainly governed by organic strength. C_b and C_p are assumed to be constant due to the strong buffer solution in bulk liquid.

3.4. Model correlations

Each component in the current modeling scheme is shown graphically in Fig 2. Any perturbation in the system input, for example the external resistance, HRT, organic feeding rate, and ambient temperature, will be directly reflected in the system output, e.g., the substrate distribution, velocity field, potential distribution and electricity generation. Thus, the multiphysics processes involving hydrodynamics, mass transport, potential distribution and chemical reactions will be dynamically simulated.

3.5. Determination of reaction order

As described in Section 3.2, Eq. (7) is actually a chain-reaction consisting of a series of elementary reactions due to the associated biochemical reactions occurring within the anodic compartment. The overall process is represented by a multi-order Butler–Volmer reaction model, whose most important parameter is the reaction order, as it correlates the species distribution to both organic removal and electricity generation. By definition, the reaction order (γ) should equal to the exponential number of the sodium acetate concentration in the reaction rate expression (Eq. (9)). Thus, the reaction order could be determined either theoretically or experimentally. The theoretical reaction order can be calculated by combining reaction rates of each elementary reaction that comprise the overall acetate oxidization. However, the elementary processes, especially those occurring inside the microbes, are so

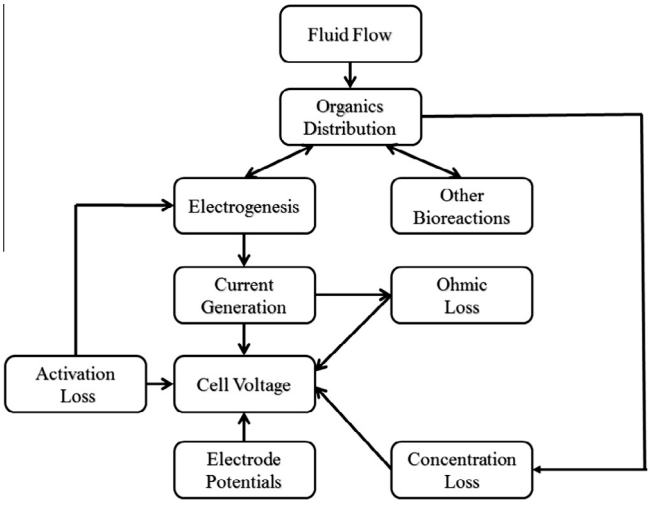

Fig. 2. Modeling scheme connecting the reaction components.

complicated that the complete reaction path of the acetate oxidization is not well understood yet.

Another approach is to use the experimental data to find the reaction order. The simplest way to determine γ is by evaluating the reaction rate at different sodium acetate concentrations, while fixing other parameters, but this is not feasible experimentally. The acetate concentration cannot be measured on the anode surface experimentally, and it is not feasible to measure organic concentration on each single point on the anode surface without affecting normal operation. The activation overpotential is not constant along with the anode surface. Due to the heterogamous distribution of acetate on the anode surface, the concentration loss in Eq. (17) also varies. Correspondingly, the activation overpotential could be different at each single point on the surface area, because electrical potential should be identical throughout the anode surface. Rate constant k, another important parameter to determine reaction rate, is controlled by the value of activation overpotential (Eq. (11)). Hence, because of the inaccessibities to acetate concentration and activation overpotential from anode surface, an alternative way should be attempted to learn the reaction order value.

Implicitly, the reaction order can be determined from numerical data by fitting to experimental data obtained from the polarization test. According to Eqs. (13)–(18), by varying the external resistance, the activation overpotential will be changed too. Consequently, the surface reaction rate (Eq. (11)) needs to be adjusted to fit this operational condition. It should be noted that the surface reaction acts as a boundary condition in species transport, and the species distribution within the anodic compartment is also changed. Eventually after a new equilibrium state is reached, the system will yield a different current generation, which is proportional to the surface reaction rate. Therefore, although implicit, the influence of the acetate concentration on the surface reaction rate could be reflected from the polarization test. A parameter estimation procedure was implemented to determine the reaction order [22,23]. The reaction order can be determined by gradually increasing the reaction order from unity to higher values and comparing the corresponding numerical data to the experimental polarization curve until there is an optimal fitting with a minimal root mean square deviation (RMSD).

4. Results and discussion

4.1. Determination of reaction order from polarization test

The results of the polarization test show that the current generation decreased from 27.3 to 4.8 mA after the external resistance was changed from 1 to 100 Ω sequentially, as shown in Fig. 3. By fitting an equation to the experimental polarization curve, the reaction order γ was estimated to be 6.4. The reaction order of 6.4 was used in the CFD simulations and the results are also shown in Fig. 3 as a symbol, with the average relative error of 7.4% between the experimental data and numerical predictions. In classical reaction kinetics, the underlying assumption that chemical reactions are triggered by collisions of activated molecules implies that the reaction order is usually below 3, as the chance of more than 3 molecules colliding simultaneously is rare. However, this does not necessarily contradict with the curve-fitted reaction order of 6.4 in the current study. On one hand microbial reaction kinetics are primarily dominated by the microbial metabolism and the electrons are generated through an NADH-NAD^+ cycle and transferred to the electrode surface via outer membrane cytochromes [24]. The reaction order of 6.4 also proves the correctness of the prior assumption that the anodic reaction is actually a chain reaction. On the other hand, the reaction order of 6.4 integrates the effects of concentration of both acetate and bacterium on reaction rate. A previous study showed the reaction rate could be determined by substrate and biomass concentration simultaneously [23] of the form:

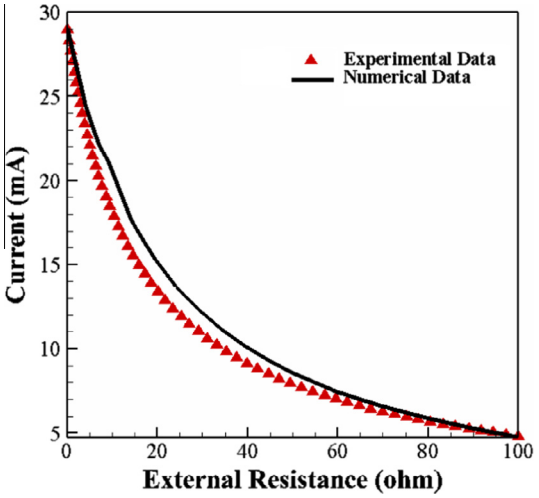

Fig. 3. Experimental polarization curve and reaction model data for current generation under varied external resistance.

$$r_a = r_{a,0} \exp\left(\frac{\alpha F}{RT}\eta_{act}\right)\frac{C_{ac}}{C_{ac}+K_{ac}}X \tag{19}$$

where X represents the concentration of biomass. The transportation, production and consumption of biomass can be solved by adding another convective–diffusion equation into the governing equations. However, the concentration of biomass cannot be easily quantified from the experiment (in an attached biofilm system). Alternatively, a power law relationship $X \sim C_{ac}^n$ is assumed to eliminate the dependence of the reaction rate on biomass concentration because theoretically, biomass is inclined to accumulate in higher substrate regions. Eq. (19) can be rewritten as:

$$r_a = r_{a,0} \exp\left(\frac{\alpha F}{RT}\eta_{act}\right)\frac{C_{ac}^{n+1}}{C_{ac}+K_{ac}} \tag{20}$$

which is the multi-order Butler–Volmer equation in the present study. The estimated reaction order will be used in the following validation tests.

4.2. Grid resolution study

To determine if the predictions are grid-independent, three grid resolutions (37 × 110, 73 × 220, and 145 × 440) are simulated and predictions of the acetate concentration and activation overpotential along the anodic surface are presented in Fig. 4A and C. With increasing grid resolution, the acetate concentration and activation overpotential slightly decreased with average relative error lower than 0.3%. However, the average relative error is still inconclusive. To quantitatively specify the numerical uncertainties and mathematical correctness of the current model, the grid convergence index (GCI) [25,26] was evaluated for the same grid resolutions (Fig. 4B and D). The error bar denotes the possible range of exact numerical solution. Clearly, the numerical solution using the fine mesh falls within the error bars with the average GCI less than 0.1%. Hence, the results from the grid resolution study indicate that a resolution of 145 × 440 is sufficient for the CFD simulation.

4.3. Reaction model validation

Two independent operations were carried out to further validate the reaction model with different organic concentrations

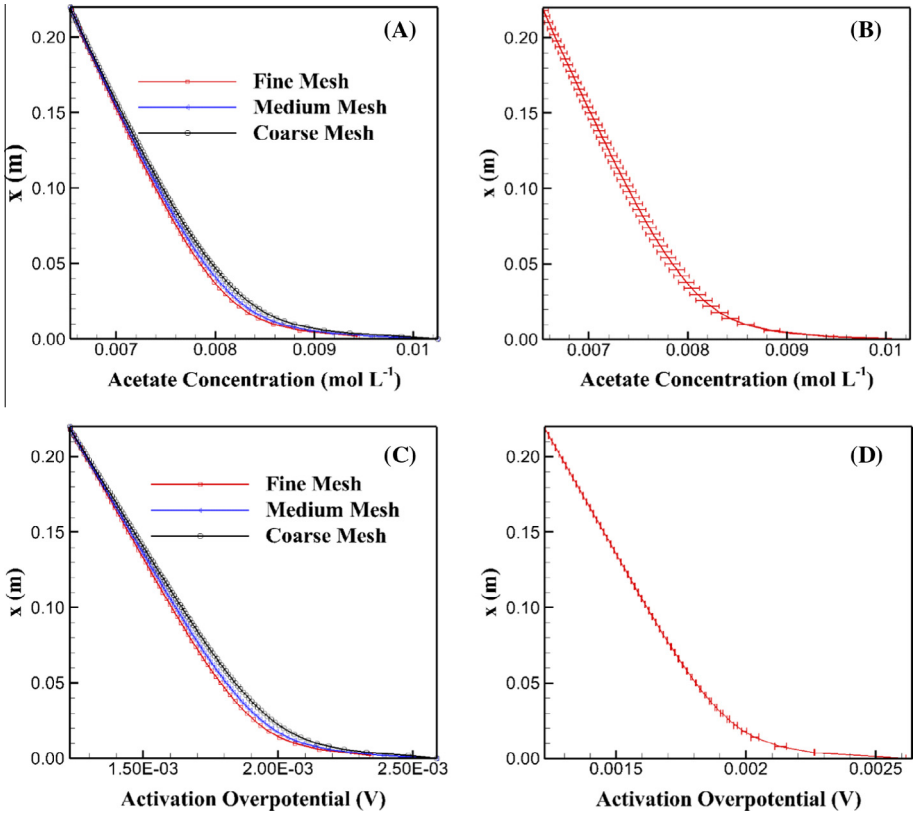

Fig. 4. Grid independent study for (A) acetate concentration using three grid resolutions; and (B) error bars on acetate concentration using grid resolution of 145 × 440; (C) activation overpotential three grid resolutions and (D) error bars on activation overpotential using grid resolution of 145 × 440.

and flow rates of the influent solution. The operating parameters remained unchanged from Section 4.2 except for the target ones being studied.

The first test reduced the influent sodium acetate concentration in three steps from 1.0 to 0.5 to 0.3 to 0.2 g L^{-1} sequentially at an anodic HRT of 10 h. Fig. 5A and B present the experimental data and CFD predictions for current generation and total COD concentration in the effluent, respectively. In general, the CFD reaction model predictions for electricity generation were in good agreement with the experiments, indicating the effectiveness of the multi-order Butler–Volmer reaction model. However, at the lowest influent sodium acetate of 0.2 g L^{-1}, a discrepancy on the effluent COD occurred between the numerical and experimental data, which might be related to the low sodium acetate concentration from the influent. The CFD model calculated the effluent COD solely based on the residual sodium acetate by neglecting the decayed biomass, but the effects of the decayed biomass could become more significant when the influent organics are low. The decayed biomass could potentially be used as substrates and/or remain in the effluent, resulting in higher COD concentrations. The time scale of such a decay-conversion process would play an important role in understanding its influence on the model prediction and warrants further investigation. Moreover, the slight discrepancy on current generation might result in an overestimation of COD removal.

Contour plots of the influent organic concentrations are shown in Fig. 6, and have been non-dimensionalized:

$$C^*_{ac} = \frac{C_{ac}}{C_{ac,0}} \tag{21}$$

where C^*_{ac} represents the nondimensional concentration of acetate, C_{ac} is the heterogeneous concentration of acetate, and $C_{ac,0}$ is the inlet acetate concentration. The organics were evenly distributed within the anodic compartment when the influent sodium acetate concentration is 1.0 g L^{-1}, and a decreased organic concentration from the influent is obtained with a lower influent organic concentration (Fig 6). The CFD predictions suggest that the anodic surface reaction occurred mainly below 13 cm after the influent organic concentration decreased to 0.2 g L^{-1}, indicating the system was not operated under the optimum condition for energy recovery.

The second test was conducted by decreasing the influent flowrate from 1.17 mL min^{-1} (anodic HRT of 5 h) to 0.59 mL min^{-1} (anodic HRT of 10 h) to 0.39 mL min^{-1} (anodic HRT of 15 h), with the influent sodium acetate concentration fixed at 0.3 g L^{-1}, to replicate the strength of traditional municipal wastewater. The CFD predictions for current generation showed satisfactory agreement with the experiments for HRT of 5 and 10 h, as shown in Fig. 7, indicating effectiveness of the multi-order reaction model on the surface reaction. However, overestimation can be seen after HRT was extended to 15 h (Fig. 7A), possibly related to two reasons. First, more substrates are consumed by non-electroactive bacteria. The tubular MFC had two PVC caps as top/bottom ends, which contained no electrode materials and would allow the growth of non-electroactive microbial community. Consumption of organic compounds in such regions could become more dominant with an extended HRT, and as a consequence, less substrate was available for electrochemically-active microorganisms. Unfortunately, such effects were not simulated by the reaction model. Second, the conventional Monod-limitation equation may not be valid to describe methanogenic activity. In this study, the volumetric reaction rate was assumed to follow conventional Monod-limitation equation, in which the reaction rate was related to the sodium acetate concentration and half-reaction constant (Eq. (6)) in a linear relationship; but actually, this could not occur ideally due to the fierce internal microbial competition with a low feeding rate. The numerical data exhibit good agreement with

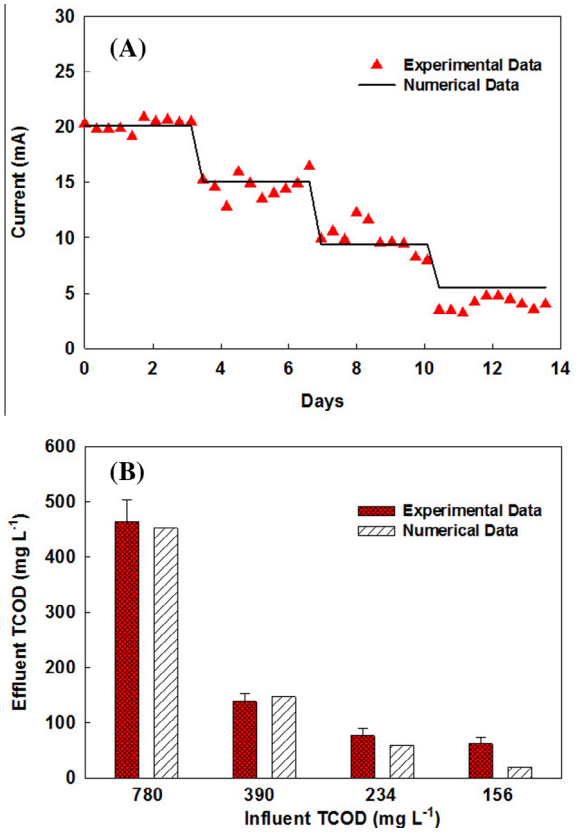

Fig. 5. Comparison of experimental and reaction model data reducing influent COD concentration from 780 to 390 to 234 to 156 mg/L sequentially: (A) current generation and (B) total COD concentration in the effluent.

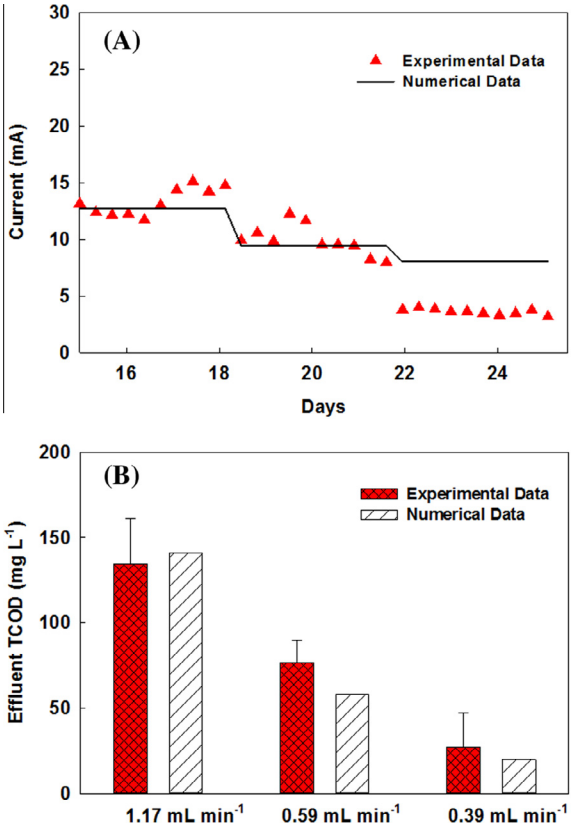

Fig. 7. Comparison of experimental and reaction model data reducing flow rate of the anolyte feeding from 1.17 to 0.59 to 0.39 mL min^{-1} sequentially: (A) current generation and (B) effluent total COD concentration.

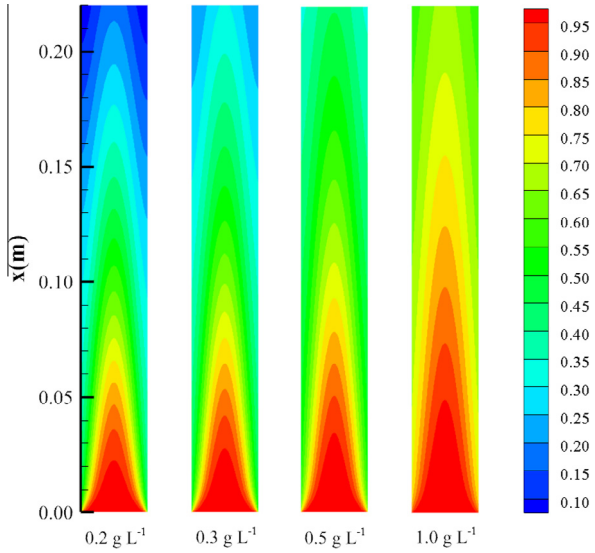

Fig. 6. Heterogeneous distribution of nondimensional acetate concentration under different influent sodium acetate concentration.

experimental data on the effluent COD concentration (Fig. 7B), and predicted that the effluent COD is 148 mg L^{-1} at anodic HRT of 5 h, comparable to 134.7 ± 26.4 mg L^{-1} obtained in the experiment. Reducing the influent feeding rate resulted in a lower effluent COD concentration, which was also predicted by the model that showed the effluent COD was reduced to 19 mg L^{-1} after the anodic HRT was extended to 15 h, within in the range of 27.3 ± 19.3 mg L^{-1} obtained from the experiments.

4.4. Perspectives

This study has demonstrated that the coupled CFD with multi-order Butler–Volmer model could effectively simulate the multi-physics (e.g., hydrodynamics, species transport, electricity generation) in the anodic chamber of a tubular MFC. Comparing to the previous MFC modeling works [27,28] that assumed homogeneous substrate distribution within anodic chamber and a constant over-potential on the anode surface, our work using a heterogeneous substrate distribution can deliver more accurate predictions for concentration loss, which in turn, affects the activation overpotential on each geometric cell. The improvement using a heterogeneous model is especially useful for predicting large-scale MFC performance because the systems are not well-mixed due to the operational limitations. Moreover, although the Butler–Volmer–Monod equation has been applied in other published MFC models to represent substrate consumption, biomass growth, and electrochemical reactivity [29–31], a multi-order model has not been used in conjunction with CFD. Thus the coupling of CFD and the multi-order Butler–Volmer model presented in this paper can be used as a platform to accommodate more diverse electron transfer mechanisms and more complex flow conditions. For example, the addition of external mediator could stimulate biomass activity and enhance electricity generation. Such an operational change can be reflected by varying the exponential number in the multi-order reaction equation. In addition, the influence of substrate type on electricity generation can also be accomplished by modifying the multi-order reaction equation. More complex hydrodynamics (e.g., tortuous internal structure, internal recirculation flow) could

be achieved by adopting geometry change from meshing process and modifying inlet and outlet boundary conditions.

Several limitations may exist in the current model and should be addressed with future work. First, like many of the previously published MFC models, real wastewater containing complex substrates and low conductivity was not considered here, resulting in discrepancies between treatment performance and model prediction. Second, the influence of biofilm (e.g. thickness, conductivity, and capacity) was not well incorporated into the model formulation. In this study, the biofilm on the anode surface was assumed as an ideal conductive material, in which the produced electrons and protons could be transported freely. Third, the current model did not involve temperature fluctuations, which may pose a significant influence on biomass activity and mass transport within the anodic compartment. This may be addressed by adding another convection diffusion equation into the governing equations. Last, biomass decay was not included in the model, and this could lead to deviations in the model predictions, especially when the organic concentration becomes low and the decayed biomass could be used as a substrate.

In addition to addressing the above limitations, further improvements may be achieved with knowledge of the electrochemically-active microorganism metabolic activities, which is necessary to determine the reaction order. A two-population microbial community could represent dominant species inside the anodic chamber, but it cannot exactly depict microbial activities. Thus, a complex bacteria community should be described in the model. Moreover, dynamic biomass attachment and detachment from the electrode surface should be considered because biomass thickness affects bacterial activity and diffusion on the substrate. Severe biomass detachment can cause operational issues, which may require a post treatment such as membrane separation process [32]. Thus, it is important to account for dynamic biofilm variation in the model. The reaction potential on the cathode surface should also be considered. For MFC applications, choosing a suitable electron acceptor for the cathode electrode is critical. Oxygen is a possible candidate due to its non-toxic and massive-available characteristics. A localized oxygen concentration can play a significant role in cathodic performance, but a high oxygen concentration may pose an unfavorable influence on the electrochemically-active microorganisms' activity, due to the cross-diffusion issue. Therefore, such a trade-off effect deserves further investigations.

5. Conclusions

A coupled CFD-multi-order Butler Volmer reaction model has been proposed and validated in the present work. Convective flow conditions and associated heterogeneous species distributions were simulated using the improved CFD reaction model. Comparing to the conventional Monod-limitation equation, the multi-order model was able to predict current generation and organics removal in a simplified way. The model was experimentally validated by varying organic concentrations and the anolyte flow rate. The CFD predictions demonstrate that the MFC system was not operated under the optimum condition for energy recovery and substrate supply could limit the anodic surface reaction in the higher zone of the reactor. Moreover, it is expected that this new model will not merely be specific to tubular MFC systems, and its application in other reactor configurations (e.g., rectangular cross-section) will be of strong interest. The model can be improved by considering more diverse microbial communities, biomass decay, complex hydrodynamic conditions and dynamic cathodic reaction potentials.

Acknowledgements

The MFC experiment of this research and J. Li was financially supported by a Grant from the National Science Foundation (#1358145). The authors acknowledge Advanced Research Computing at Virginia Tech (http://www.arc.vt.edu) for providing computational resources and technical support that have contributed to the results reported within this paper.

Appendix A. Supplementary data

Supplementary data associated with this article can be found, in the online version, at http://dx.doi.org/10.1016/j.cej.2016.03.110.

References

[1] W.W. Li, H.Q. Yu, Z. He, Towards sustainable wastewater treatment by using microbial fuel cells-centered technologies, Energy Environ. Sci. 7 (2014) 911–924.
[2] L. Xu, Y.Q. Zhao, L. Doherty, Y.S. Hu, X.D. Hao, The integrated processes for wastewater treatment based on the principle of microbial fuel cells: a review, Crit. Rev. Environ. Sci. Technol. 46 (2016) 60–91.
[3] H. Liu, R. Ramnarayanan, B.E. Logan, Production of electricity during wastewater treatment using a single chamber microbial fuel cell, Environ. Sci. Technol. 38 (2004) 2281–2285.
[4] S. You, Q. Zhao, J. Zhang, J. Jiang, S. Zhao, A microbial fuel cell using permanganate as the cathodic electron acceptor, J. Power Sources 162 (2006) 1409–1415.
[5] Z. He, N. Wagner, S.D. Minteer, L.T. Angenent, An upflow microbial fuel cell with an interior cathode: assessment of the internal resistance by impedance spectroscopy, Environ. Sci. Technol. 40 (2006) 5212–5217.
[6] F.J. Hernández-Fernández, A. Pérez de los Ríos, M.J. Salar-García, V.M. Ortiz-Martínez, L.J. Lozano-Blanco, C. Godínez, F. Tomás-Alonso, F. Quesada-Medina, Recent progress and perspectives in microbial fuel cells for bioenergy generation and wastewater treatment, Fuel Process Technol. 138 (2015) 284–297.
[7] K. Rabaey, P. Clauwaert, P. Aelterman, W. Verstraete, Tubular microbial fuel cells for efficient electricity generation, Environ. Sci. Technol. 39 (2005) 8077–8082.
[8] H. Sun, S. Luo, R. Jin, Z. He, Multitask lasso model for investigating multimodule design factors, operational factors, and covariates in tubular microbial fuel cells, ACS Sustainable Chem. Eng. 3 (2015) 3231–3238.
[9] F. Zhang, K.S. Jacobson, P. Torres, Z. He, Effects of anolyte recirculation rates and catholytes on electricity generation in a litre-scale upflow microbial fuel cell, Energy Environ. Sci. 3 (2010) 1347–1352.
[10] K.S. Jacobson, P.T. Kelly, Z. He, Energy balance affected by electrolyte recirculation and operating modes in microbial fuel cells, Water Environ. Res. 87 (2015) 252–257.
[11] V.M. Ortiz-Martínez, M.J. Salar-García, A.P. de los Ríos, F.J. Hernández-Fernández, J.A. Egea, L.J. Lozano, Developments in microbial fuel cell modeling, Chem. Eng. J. 271 (2015) 50–60.
[12] S. Luo, H. Sun, Q. Ping, R. Jin, Z. He, A review of modeling bioelectrochemical system (BES): engineering and statistical aspects, Energies 9 (2016) 1–27.
[13] R. González-Cabaleiro, J.M. Lema, J. Rodríguez, Metabolic energy-based modelling explains product yielding in anaerobic mixed culture fermentations, PLoS ONE 10 (2015) e0126739.
[14] C. Picioreanu, M.C.M. van Loosdrecht, T.P. Curtis, K. Scott, Model based evaluation of the effect of pH and electrode geometry on microbial fuel cell performance, Bioelectrochemistry 78 (2010) 8–24.
[15] C.T. Wang, C.K. Shaw, T.Y. Hu, Optimization of flow in microbial fuel cells: an investigation into promoting micro-mixer efficiency with obstacle, Tamkang J. Sci. Eng. 14 (2011) 25–31.
[16] J.R. Kim, H.C. Boghani, N. Amini, K.F. Aguey Zinsou, I. Michie, R.M. Dinsdale, A.J. Guwy, Z.X. Guo, G.C. Premier, Porous anodes with helical flow pathways in bioelectrochemical systems: the effects of fluid dynamics and operating regimes, J. Power Sources 213 (2012) 382–390.
[17] I.S. Michie, J.R. Kim, R.M. Dinsdale, A.J. Guwy, G.C. Premier, The influence of anodic helical design on fluid flow and bioelectrochemical performance, Bioresour. Technol. 165 (2014) 13–20.
[18] B. Kim, H. Kim, J. Kim, J. Yu, Computational fluid dynamic analysis in microbial fuel cells with different anode configurations, Water Sci. Technol. 69 (2014) 1447–1452.
[19] A. Vila-Rovira, S. Puig, M.D. Balaguer, J. Colprim, Anode hydrodynamics in bioelectrochemical systems, RSC Adv. 5 (2015) 78994–79000.
[20] B.E. Logan, B. Hamelers, R. Rozendal, U. Schröder, J. Keller, S. Freguia, P. Aelterman, W. Verstraete, K. Rabaey, Microbial fuel cells: methodology and technology, Environ. Sci. Technol. 40 (2006) 5181–5192.
[21] C. Picioreanu, I.M. Head, K.P. Katuri, M.C.M. van Loosdrecht, K. Scott, A computational model for biofilm-based microbial fuel cells, Water Res. 41 (2007) 2921–2940.

[22] N.E. Stein, H.M. Hamelers, G. van Straten, K.J. Keesman, On-line detection of toxic components using a microbial fuel cell-based biosensor, J. Process Control 22 (2012) 1755–1761.
[23] Y. Zeng, Y.F. Choo, B.H. Kim, P. Wu, Modelling and simulation of two-chamber microbial fuel cell, J. Power Sources 195 (2010) 79–89.
[24] D.R. Lovley, The microbe electric: conversion of organic matter to electricity, Curr. Opin. Biotechnol. 19 (2008) 564–571.
[25] P.J. Roache, Perspective: a method for uniform reporting of grid refinement studies, J. Fluid Eng. 116 (1994) 405–413.
[26] I.B. Celik, U. Ghia, P.J. Roache, Procedure for estimation and reporting of uncertainty due to discretization in CFD applications, J. Fluid Eng. T. ASME 130 (2008).
[27] Q. Ping, C. Zhang, X. Chen, B. Zhang, Z. Huang, Z. He, Mathematical model of dynamic behavior of microbial desalination cells for simultaneous wastewater treatment and water desalination, Environ. Sci. Technol. 48 (2014) 13010–13019.
[28] J. Li, Z. He, Development of a dynamic mathematical model for membrane bioelectrochemical reactors with different configurations, Environ. Sci. Pollut. Res. 23 (2015) 3897–3906.
[29] L. Zhao, J. Brouwer, J. Naviaux, A. Hochbaum, Modeling of polarization losses of a microbial fuel cell, in: ASME 2014 12th International Conference on Fuel Cell Science, Engineering and Technology collocated with the ASME 2014 8th International Conference on Energy Sustainability, American Society of Mechanical Engineers, 2014.
[30] M. Yan, L. Fan, Constant voltage output in two-chamber microbial fuel cell under fuzzy PID control, Int. J. Electrochem. Sci. 8 (2013) 3321–3332.
[31] H. Huang, X. Wang, X. Gong, S. You, Numerical anodic mass transfer of redox mediators in microbial fuel cell, in: 2013 International Conference on Materials for Renewable Energy and Environment (ICMREE), IEEE, 2014, pp. 298–302.
[32] J. Li, G. Rosenberger, Z. He, Integrated experimental investigation and mathematical modeling of a membrane bioelectrochemical reactor with an external membrane module, Chem. Eng. J. 287 (2016) 321–328.